Supporting Information

A Zn(II)-Based Metal–Organic Framework Constructed from Cyclotriphosphazene Hexacarboxylate and π-Conjugated Bisterpyridine Ligands for Dual Applications in Dye Photodegradation and VOC Sensing

Elif Özcan*

Contents

Table S7. Comparison of dye degradation of **PCP-35** with representative Zn-based and phosphazene-related MOFs.

Section S1. Instrumentation and Materials

All solvents, zinc nitrate salt ($Zn(NO_3)_2 \cdot 6H_2O$), and organic reagents were purchased from commercial suppliers in analytical grade and used directly without further purification. Hexachlorocyclotriphosphazene ($N_3P_3Cl_6$) was obtained from BLDpharm and employed as the starting precursor. The cyclotriphosphazene-based hexacarboxylic acid ligand (**H_6L**) was synthesized according to a modified literature method.[1]

Fourier-transform infrared (FT-IR) spectra were measured using a PerkinElmer 100 spectrometer in the 600–4000 cm^{-1} region. Thermal behavior was evaluated on a Mettler Toledo TGA/SDTA851e instrument under airflow at a heating rate of 10 °C min^{-1}. Powder X-ray diffraction (PXRD) data were collected on a Bruker D8 Advance diffractometer with Cu Kα radiation (λ = 1.5406 Å), operated at 40 kV and 40 mA, scanning from 2θ = 2° to 50° at 6° min^{-1}. Morphological features were examined by field-emission scanning electron microscopy (JEOL JSM-7800F). Solid-state photoluminescence spectra were recorded at room temperature using a Varian Cary Eclipse spectrofluorometer with a fixed slit width, on finely ground samples of approximately 10 mg. Electron paramagnetic resonance (EPR) measurements were performed on a JEOL JES-FA300 spectrometer to investigate the presence of paramagnetic species.

Single crystals of **PCP-35** suitable for X-ray diffraction were obtained under solvothermal conditions. Data were collected on a Bruker APEXII CCD diffractometer with Mo Kα radiation (λ = 0.71073 Å). Data indexing, integration, and reduction[2] were performed using the APEX2[3] software suite, and absorption corrections[4] were applied. The structure was solved using SHELXT[5] and refined by full-matrix least-squares techniques on F^2 with SHELXL[6] within the Olex2 environment[7]. PLATON analysis revealed a total solvent-accessible void volume of 1727.1 $Å^3$ per unit cell, corresponding to 28.0% of the unit cell volume (6177.8 $Å^3$). The diffuse electron density arising from highly disordered solvent molecules could not be modeled explicitly; therefore, the SQUEEZE[8] routine was applied to remove this contribution. The masked solvent-accessible regions were consistent with the presence of disordered guest molecules, in agreement with thermogravimetric analysis (TGA) results. The crystallographic data and refinement details for **PCP-35** are summarized in Table S3. Topological analysis was performed using theToposPro program[9]. The validated structure has been deposited in the Cambridge Crystallographic Data Centre under deposition number CCDC 2369902 and may be obtained through the CCDC website www.ccdc.cam.ac.uk/deposit.

Synthesis of Hexapodal Ligand (H_6L) and N-Divergent Donor

S1.1. Synthesis of Hexapodal Ligand (H_6L)

In a typical procedure, potassium carbonate (20.75 mmol, 2.88 g) was added to a 30 mL solution of anhydrous acetone containing methyl 4-hydroxybenzoate (12.10 mmol, 1.84 g) and hexachlorocyclotriphosphazene ($P_3N_3Cl_6$, 2.88 mmol, 1.0 g). The reaction mixture was maintained under stirring at 80 °C overnight. After solvent removal under reduced pressure, the resulting solid residue was dissolved in 50 mL dichloromethane. The organic extract was subsequently washed with water, dried over anhydrous Na_2SO_4, and concentrated again under vacuum. This yielded the

intermediate ligand **H_6L-E** as a white powder in 95% yield (2.85 g, calculated with respect to $P_3N_3Cl_6$). The compound was confirmed by mass spectrometry, ^{1}H NMR, and ^{31}P NMR: MALDI-TOF (m/z): [M^+] = 1040.31; ^{1}H NMR (500 MHz, $CDCl_3$, ppm): δ 7.87 (d, 12H, Ar–H), 7.01 (d, 12H, Ar–H), 3.94 (s, 18H, –OCH_3); ^{31}P NMR (202 MHz, $CDCl_3$, ppm): δ 7.53 (s).

For hydrolysis, sodium hydroxide (27.84 mmol, 1.11 g) was dissolved in 75 mL of methanol and added to **H_6L-E** (1.92 mmol, 2.0 g). The mixture was heated at 80 °C overnight with continuous stirring. After evaporation of the solvent, the residue was dissolved in water, filtered, and acidified with dilute HCl to adjust the pH to approximately 2–3. A white solid precipitated, which was isolated by filtration, washed thoroughly with water, and dried to afford the target ligand **H_6L** in 97.4% yield (1.79 g). The structure was verified by MALDI-TOF, NMR, and IR spectroscopy: MALDI-TOF (m/z): [M^+] = 956.26; ^{1}H NMR (500 MHz, DMSO-d_6, ppm): δ 7.83 (d, 12H, Ar–H), 7.00 (d, 12H, Ar–H); ^{31}P NMR (202 MHz, DMSO-d_6, ppm): δ 7.99 (s). IR (ATR, cm^{-1}): 3081.4, 2952.2, 2666.6, 2537.0, 2103.7, 1692.7, 1601.7, 1504.7, 1421.9, 1312.9, 1276.1, 1257.5, 1209.4, 1200.3, 1184.2, 1156.2, 1016.7, 980.5, 942.7, 894.8, 879.0, 858.4, 816.2, 801.1, 771.4, 735.5, 717.0, 689.6, 652.9.

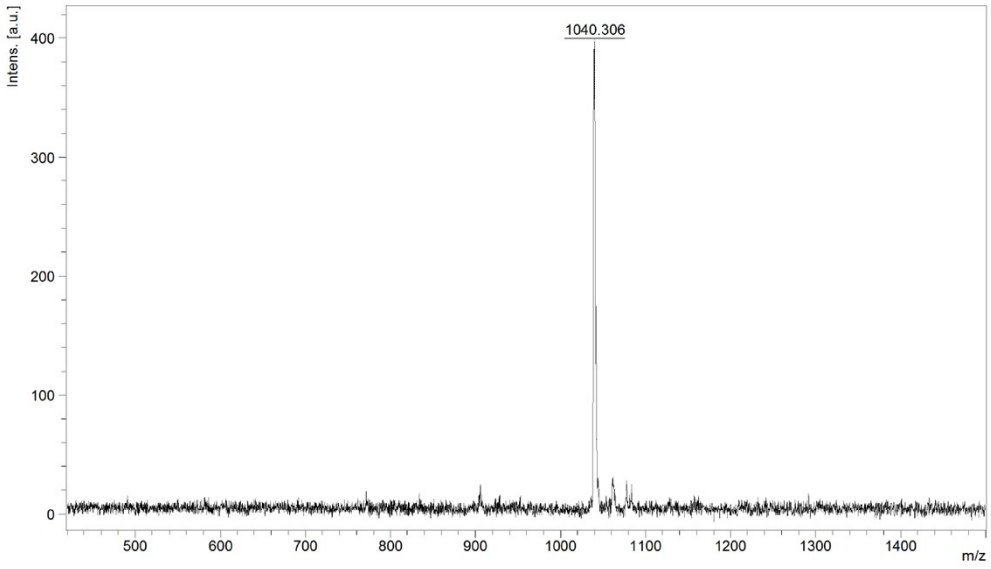

Figure S1. Mass spectrum of **H_6L-E**.

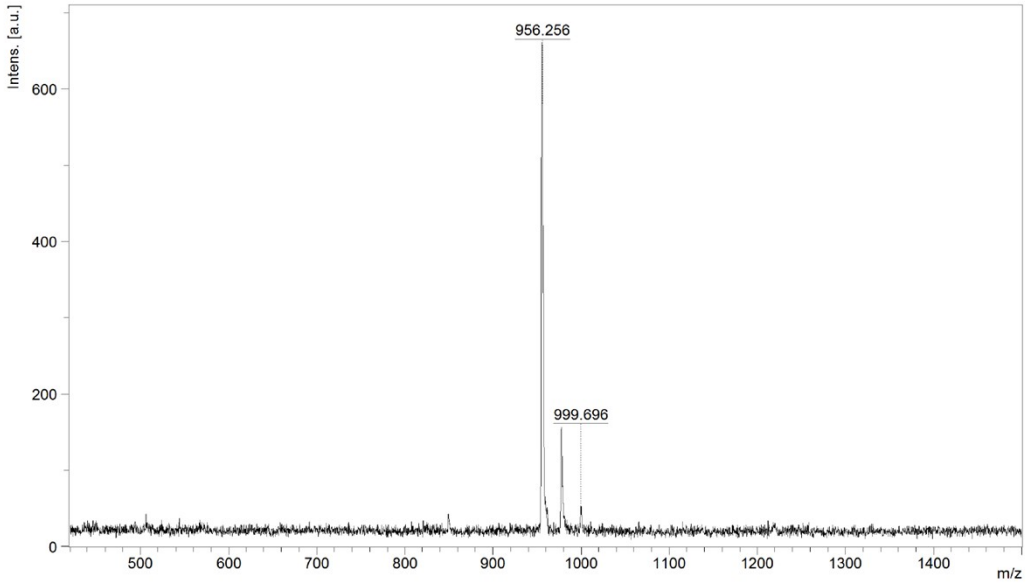

Figure S2. Mass spectrum of $\mathbf{H_6L}$.

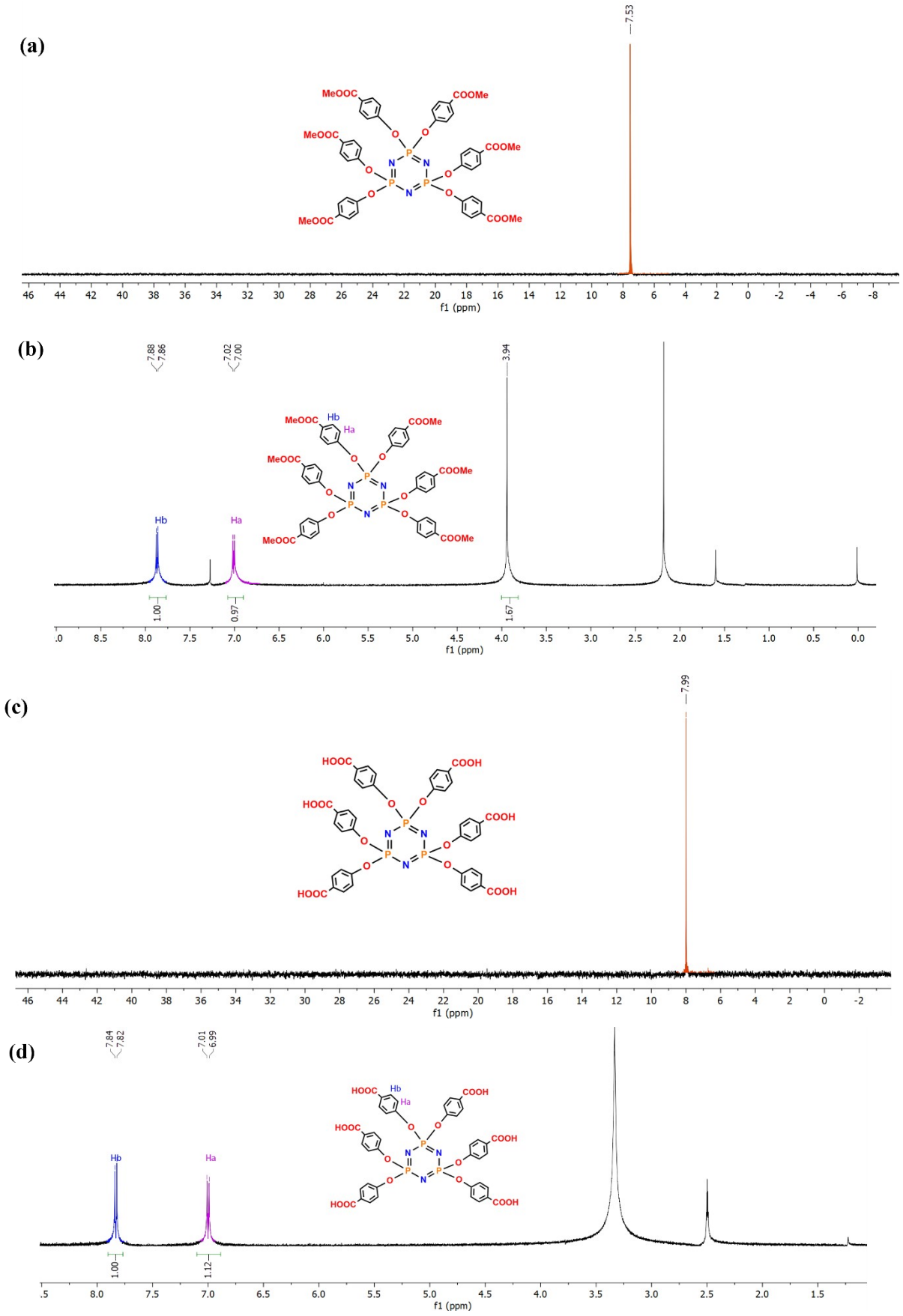

Figure S3. ^{31}P NMR and ^{1}H NMR spectrum of **H_6L-E** and **H_6L**.

S1.2. Synthesis and Characterization of 1,4-Bis(2,2′:6′,2″-terpyridin-4′-yl)benzene (bisterp)

The compound was synthesized following a reported procedure[10]. Terephthalaldehyde (0.2764 g, 2.1 mmol), 15% KOH solution (2.9 mL), and NH_4OH (29 mL) were dissolved in 32 mL of methanol (CH_3OH). Subsequently, 2-acetylpyridine (1.00 g, 8.3 mmol) was added to the solution. The mixture was refluxed at the boiling point of methanol for 3 days under continuous stirring. The resulting yellow precipitate was collected by vacuum filtration, washed three times with distilled water, and then dissolved in 40 mL of chloroform ($CHCl_3$). The organic phase was extracted with water (3 × 30 mL), dried over anhydrous Na_2SO_4, and filtered. After solvent evaporation of the filtrate, the bis(terpyridine) product (0.60 g, 46%) was obtained as a pure solid. The structure of the compound was confirmed by ^1H NMR spectroscopy ($CDCl_3$, 298 K). The proton signals appeared at δ = 8.81, 8.77, 8.70, 8.07, 7.91, and 7.38 ppm, with integration values consistent with the proposed structure (Spectrum 21)**.**

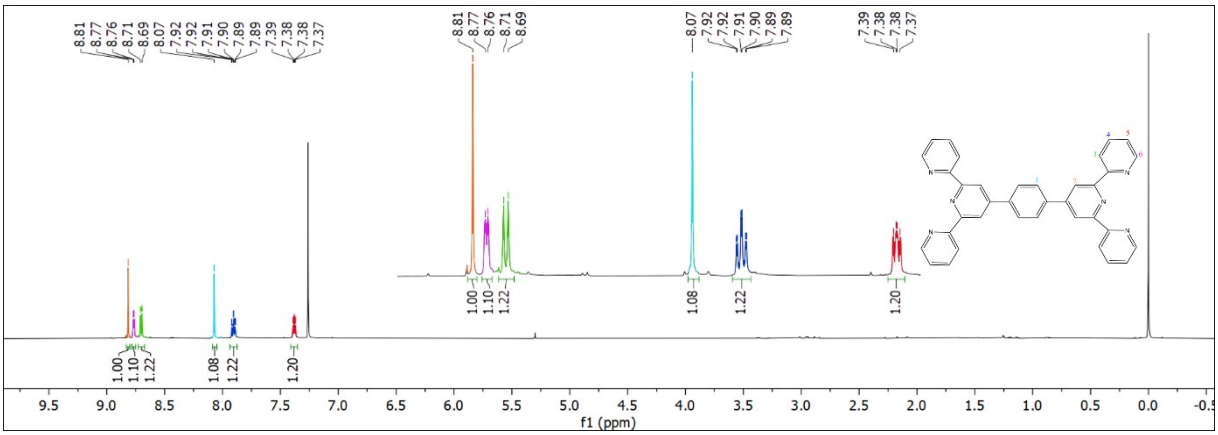

Figure S4. ^1H NMR spectrum of the bis(terpyridine) compound.

S1.3. Photocatalytic Reaction Measurements

Photocatalytic activity tests were performed under ambient conditions using a 250 mL borosilicate glass reactor. A Xenon lamp system (OPT-S500F) fitted with a UV–IR cutoff filter (λ > 420 nm) was utilized to generate visible light irradiation within the 420–780 nm range. The light intensity measured at the surface of the reaction solution was 41.4 mW cm^{-2}. In a typical experiment, 100 mL of dye solution (30 ppm) was combined with 30 mg of the freshly prepared MOF sample. The suspension was magnetically stirred in the dark for 30 minutes to allow adsorption–desorption equilibrium. Afterwards, the mixture was exposed to visible light irradiation while stirring was maintained. At predetermined intervals, 4 mL aliquots were withdrawn, and the catalyst was removed by centrifugation. The concentration of the residual dyes was monitored using a Shimadzu UV-1900i spectrophotometer by measuring absorbance at the characteristic maximum wavelengths of each dye (MB: 665 nm, RhB: 554 nm, MO: 463 nm). Solutions with initial concentrations between 4 and 20 mg L^{-1} were also prepared to evaluate the effect of concentration, and catalyst loadings were varied to optimize the degradation efficiency. The optimum parameters were found to be 100 mL solution volume, catalyst dosage of 200 mg L^{-1}, and pH values in the range of 5.0–6.0 depending on the dye. All measurements were conducted at 25 ± 2 °C. The degradation kinetics were analyzed using a pseudo-first-order model according to the following equation:

$$ln(C_0/C) = kt \quad (1)$$

where C_0 is the initial dye concentration, C is the concentration at time t, and k is the apparent rate constant.

The EPR behavior of the **PCP-35** photocatalyst was investigated using TEMPO (2,2,6,6-tetramethyl-1-piperidinyloxy) as the spin-trapping agent. To detect the generation of $O_2^{\bullet-}$ radicals, a suspension was prepared by dispersing 15 mg of **PCP-35** in 50 mL of a water–methanol mixture, followed by the addition of TEMPO at a concentration of 0.05 mol/L. The spectra were recorded at 25 °C, initially under dark conditions (0 min) and subsequently after 5 minutes of light irradiation.

S1.4. Electrochemical Analysis

Electrochemical studies were conducted on a Metrohm Autolab PGSTAT204 potentiostat–galvanostat system controlled with NOVA 2.1 software, employing a conventional three-electrode arrangement. Cyclic voltammetry (CV) was carried out in a 0.5 M H_2SO_4 electrolyte to assess the catalytic activity of the prepared coordination polymers (CPs). A glassy carbon electrode (GCE) served as the working electrode, while Ag/AgCl and a platinum wire were used as reference and counter electrodes, respectively. For electrode modification, catalyst ink was formulated by dispersing the sample in ethanol and adding a 5 wt% Nafion solution as a binder. CV profiles were initially recorded for the bare GCE, followed by measurements using the catalyst-coated GCE to evaluate electrocatalytic enhancement. Electrochemical impedance spectroscopy (EIS) experiments were performed under the same electrode configuration in potentiostatic mode, within the frequency range of 0.10 Hz–4 kHz, using a sinusoidal perturbation of 0.07 V.

To gain insight into the electronic band structure relevant to photocatalysis, the conduction band (CB) and valence band (VB) edge positions of **PCP-35** were estimated. Flat band potentials were derived from Mott–Schottky (MS) analysis and subsequently converted to the normal hydrogen electrode (NHE) scale using Equation (3). VB energies were then calculated by adding the optical band gap (E_g), obtained from Tauc plot analysis, to the CB values as shown in Equation (4). These electrochemical evaluations provide essential information on the redox characteristics and charge-transfer pathways of the CPs, clarifying their role in photocatalytic activity and efficiency.

$$E(NHE) = E(Ag/AgCl) + 0.197 \quad (3)$$

$$E_{VB} = E_{CB} + Eg \quad (4)$$

Electrode Preparation

For both CV and EIS measurements, catalyst inks were prepared by suspending 1 mg of the material in 1 mL of ethanol and adding 20 µL of 5 wt% Nafion solution. The mixture was homogenized by sonication or vortexing until a uniform suspension was obtained. Then, 15 µL of the dispersion was drop-cast onto the surface of a pre-polished glassy carbon electrode using a micropipette. The electrodes were allowed to dry at room temperature to ensure solvent evaporation before electrochemical testing.

S2. Characterization Details

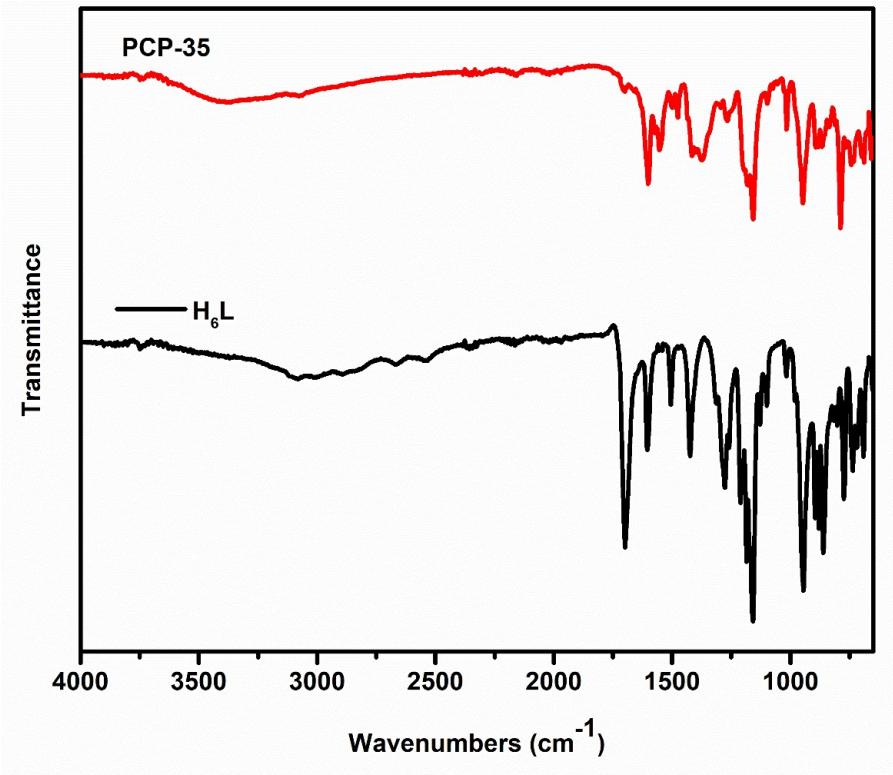

Figure S5. FTIR spectra of **PCP-35** and **H_6L**.

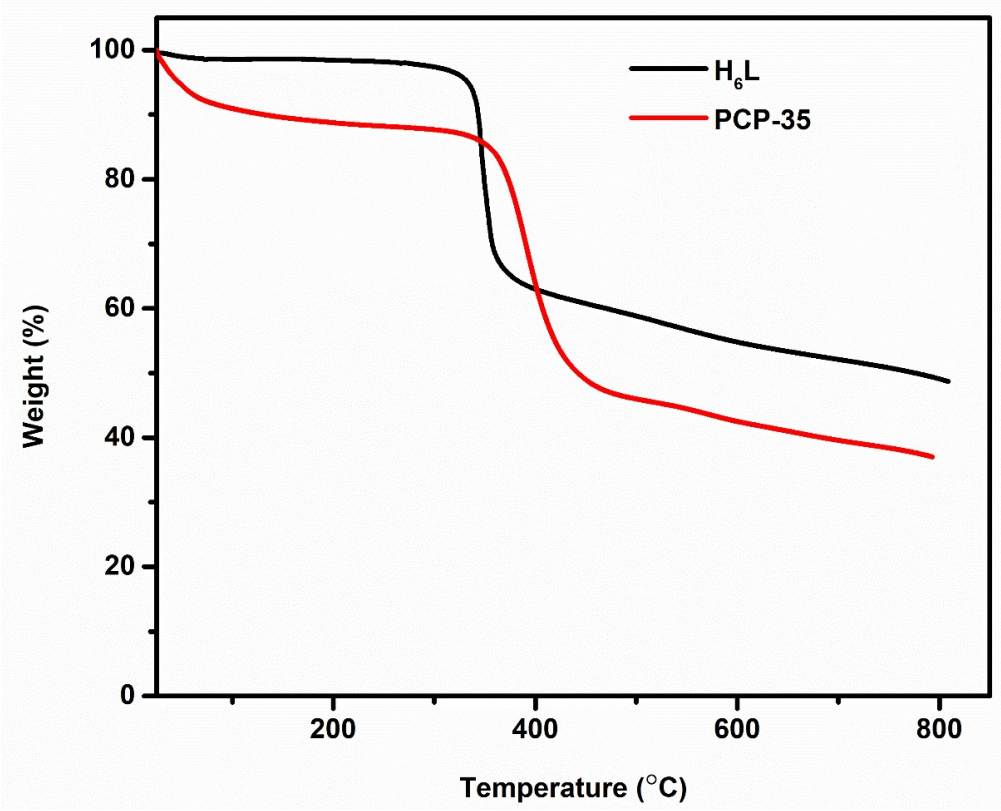

Figure S6. Thermal Analysis curves (TGA) of **PCP-35** and **H_6L**.

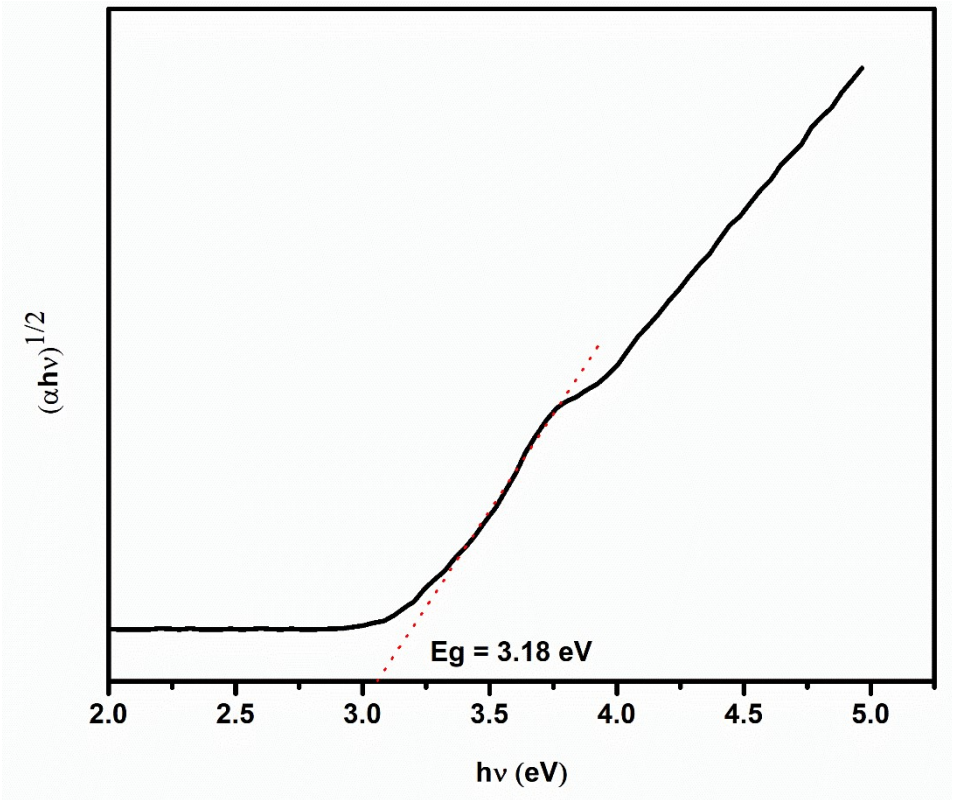

Figure S7. (a) Kubelka-Munk Plot of **PCP-35.**

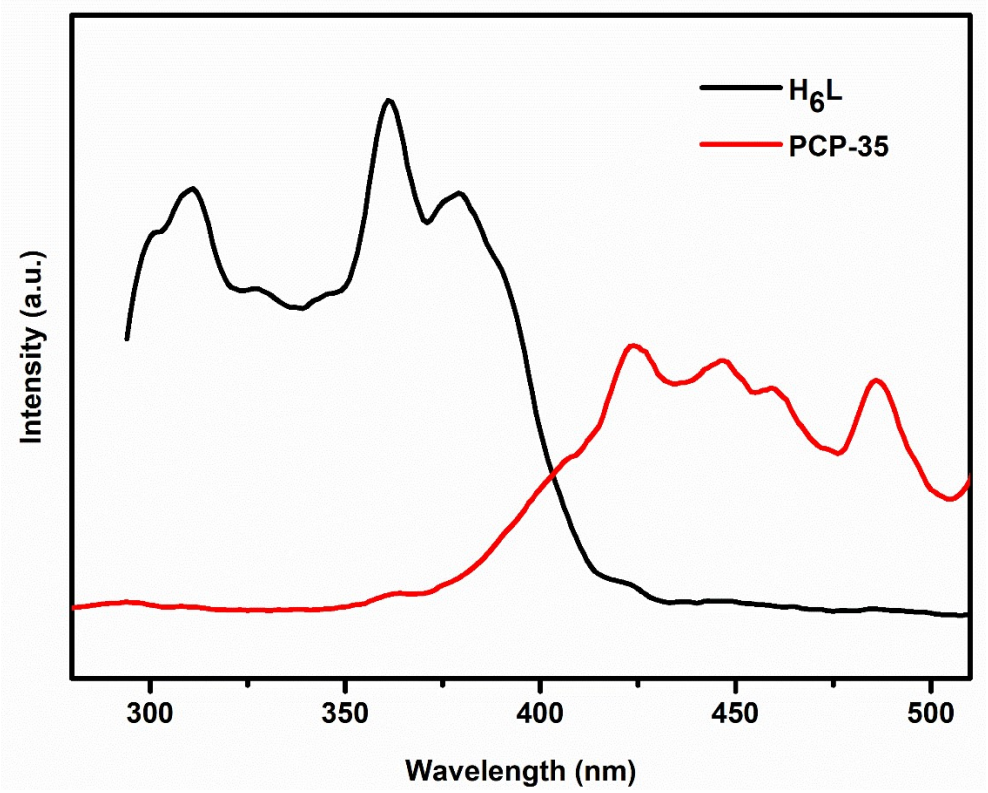

Figure S8. The solid-state emission spectra of the ligand **H_6L** and **PCP-35** at room temperature.

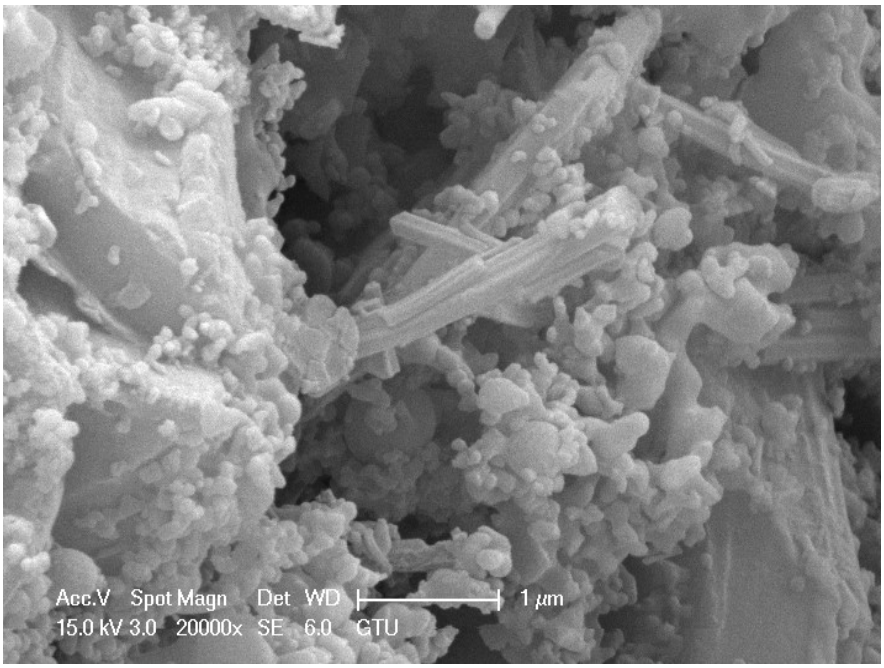

Figure S9. SEM image of **PCP-35.**

Section S3. Photocatalytic and Electrochemical Studies

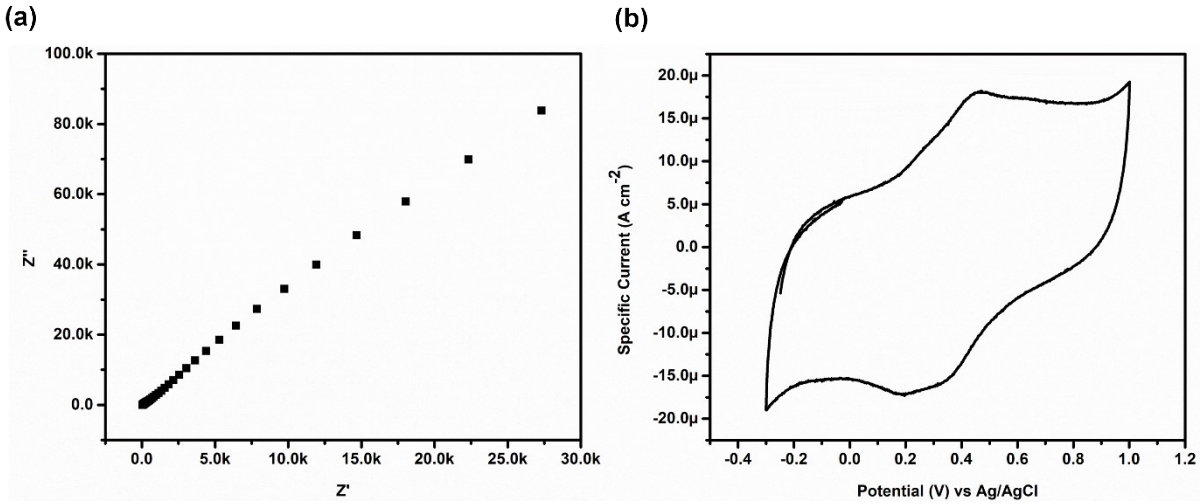

Figure S10. EIS (a) and CV (b) graph of **PCP-35**.

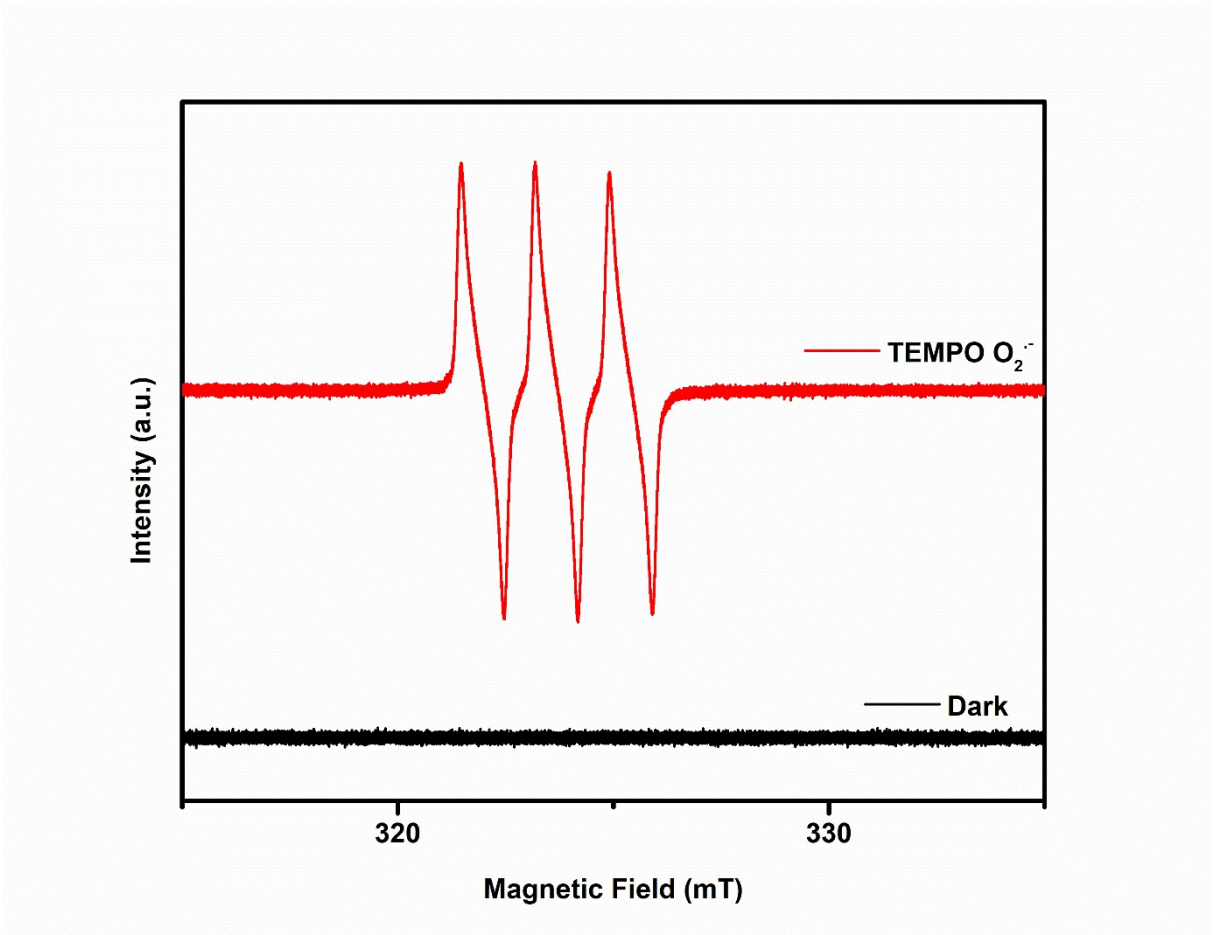

Figure S11. EPR detection of $O_2^{\cdot-}$ radical of **PCP-35** catalyst.

Table S1. Pseudo-First-Order Kinetic Parameters.

Dye	k (min^{-1})	R^2
MB	0.076	0.997
MO	0.040	0.987
RhB	0.035	0.976

Table S2. Calculated TON and TOF values for the photocatalytic degradation of dyes by **PCP-35** under visible-light irradiation.

Dye	Initial concentration	Volume	Catalyst amount	Degradation (%)	Time (min)	TON	TOF (h^{-1})
MB	30 ppm	100 mL	30 mg	96	40	0.205	0.306
MO	30 ppm	100 mL	30 mg	91	60	0.190	0.190
RhB	30 ppm	100 mL	30 mg	89	60	0.127	0.127

Note: TON and TOF values were calculated based on the experimentally observed degradation efficiencies using the empirical formula of **PCP-35**, $C_{128}H_{108}N_{19}O_{29}P_3Zn_4$ (formula weight = 2730.72 g mol^{-1}), assuming that all Zn(II) centers act as catalytically accessible active sites.

$$TON = \frac{moles\ of\ degraded\ dye}{moles\ of\ Zn\ active\ sites} \qquad TOF = \frac{TON}{reaction\ time\ (h)}$$

Section S4. Fluorescence Sensing Experiments

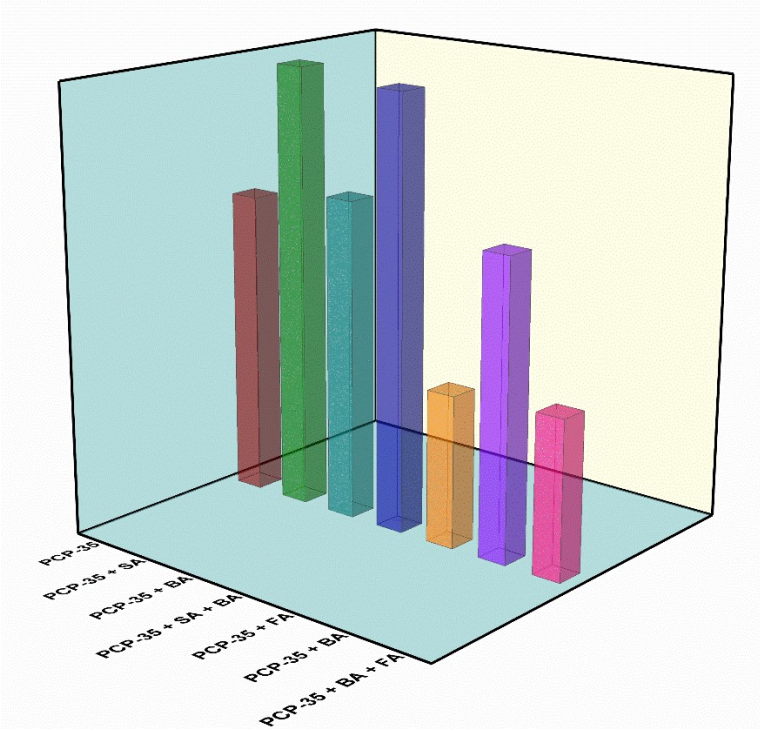

Figure S12. The interference experiments of benzaldehyde on the detection of salicylaldehyde and furfural in **PCP-35**.

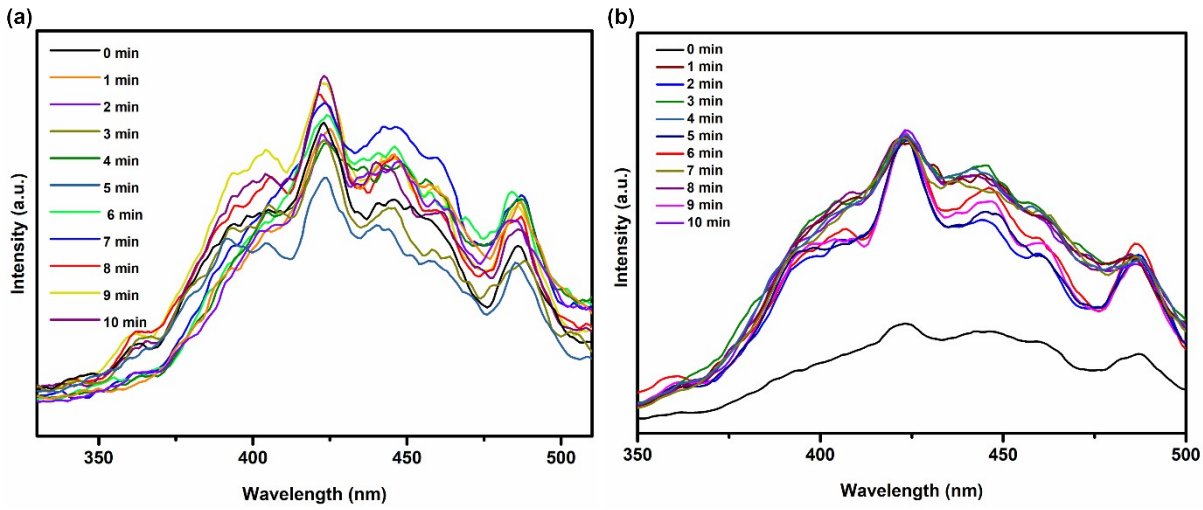

Figure S13. (a) Time-dependent emission spectrum for **PCP-35** in three aldehydes together. (b) Time-dependent emission spectrum for **PCP-35** in the p-hydroxybenzaldehyde.

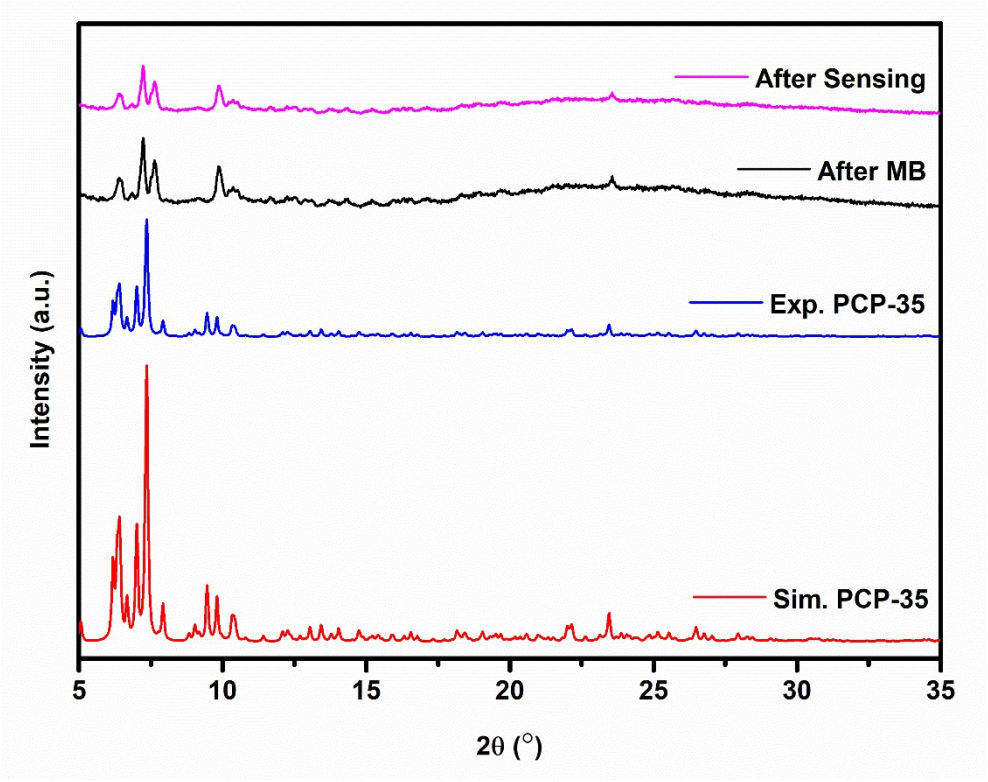

Figure S14. PXRD patterns of **PCP-35**, before and after PC and sensing VOCs.

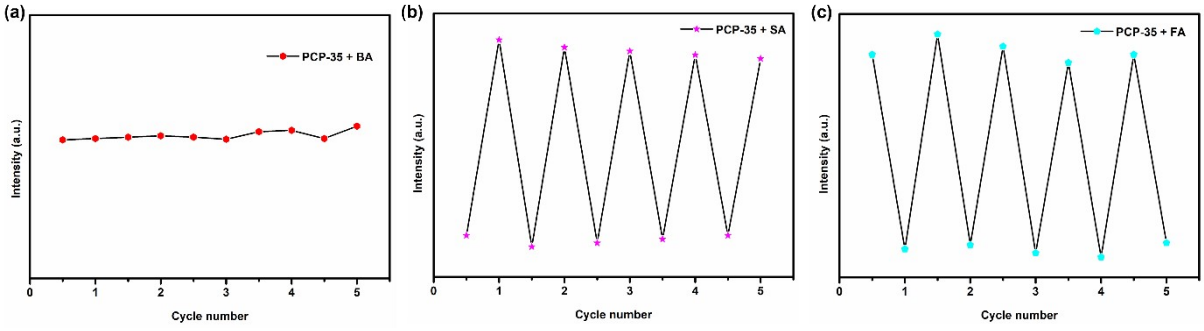

Figure S15. Recyclability test of **PCP-35** detecting aldehyde vapors: (a) benzaldehyde; (b) salicylic aldehyde, (c) furfural.

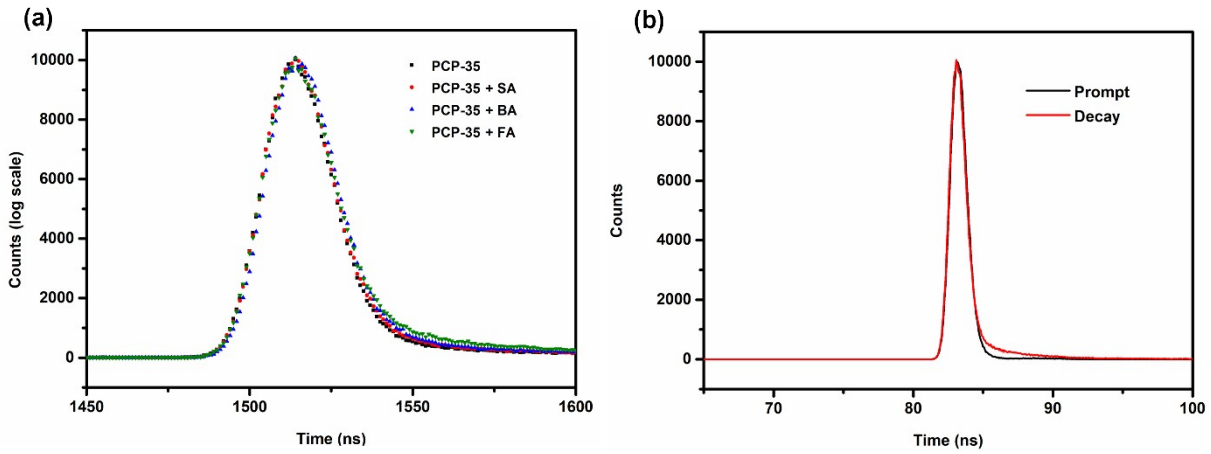

Figure S16. The lifetimes of **PCP-35** and aldehydes.

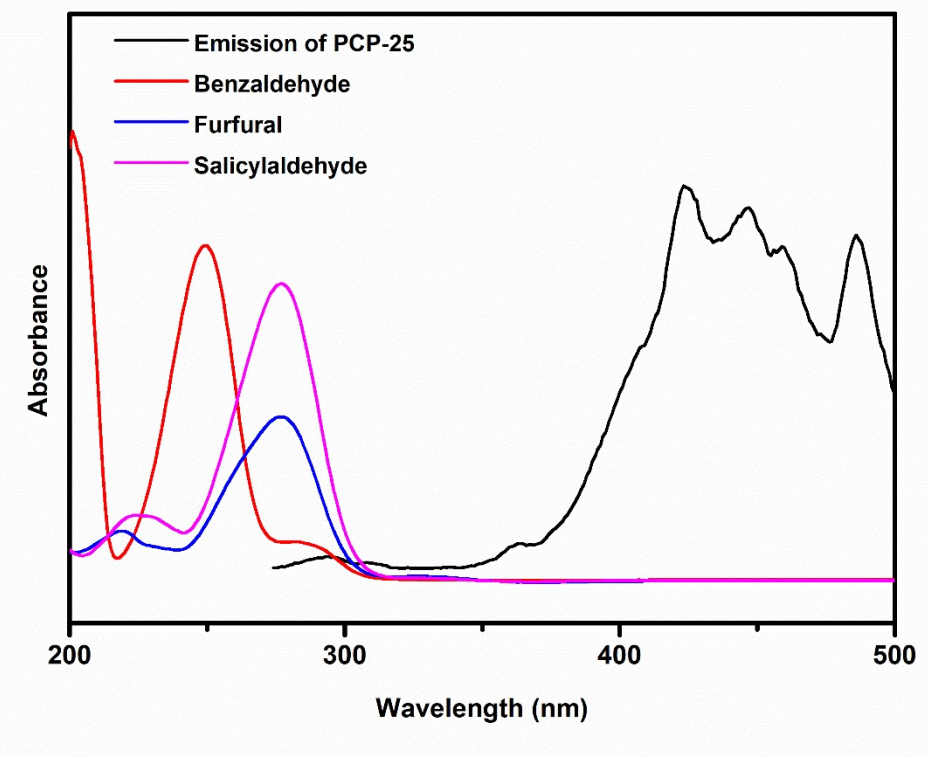

Figure S17. Spectral overlap between the emission spectrum of **PCP-25** (λ_{ex} = 275 nm) and the absorption spectra of aldehyde analytes investigated.

Section S5. Crystallographic Data and Structural Information

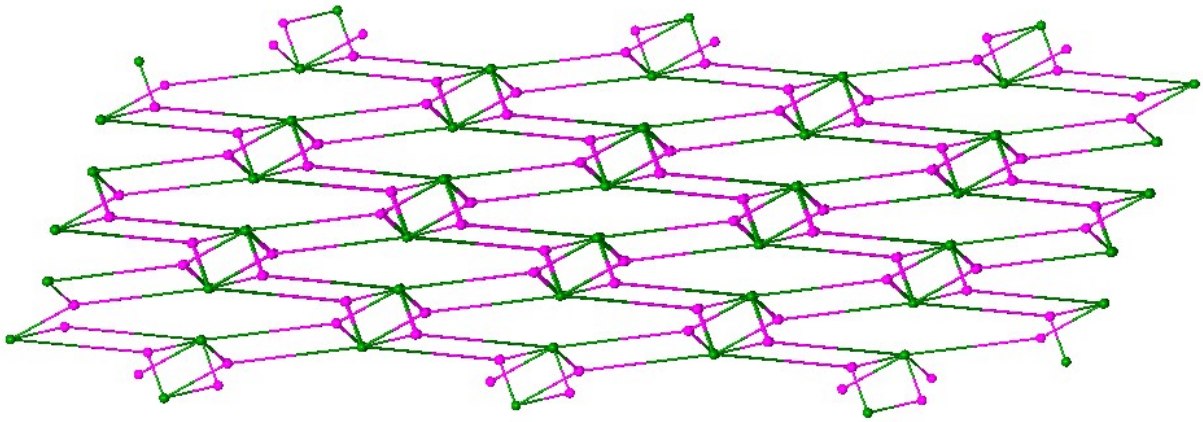

Figure S18. Topological representation of **PCP-35** derived from ToposPro analysis.

Table S3. Single crystal structure data for **PCP-35**.

Identification code	**CCDC2369902**
empirical formula	$C_{128}H_{108}N_{19}O_{29}P_3Zn_4$
formula weight	2730.72
temperature/K	298
crystal system	triclinic
space group	P-1
a/Å	14.750 (1) Å
b/Å	18.5661 (13) Å
c/Å	24.1716 (18) Å
α/°	89.065 (3)°
β/°	83.323 (3)°
γ/°	70.045 (3)°
volume/Å^3	6177.8 (8)
Z	2
ρ_{calc}g/cm^3	1.468
μ/mm^{-1}	0.891
F(000)	2812
crystal size/mm^3	0.22 × 0.18 × 0.15
2Θ range for data collection/°	2.92–50.292
index ranges	$-17 \leq h \leq 17$, $-22 \leq k \leq 22$, $-28 \leq l \leq 28$
reflections collected	117279
independent reflections	22037 [R_{int} = 0.1061, R_{sigma} = 0.1070]
data/restraints/parameters	22037/1147/1424
goodness-of-fit on F^2	0.986
final R indexes [I>=2σ (I)]	R_1 = 0.0644, wR_2 = 0.1680
final R indexes [all data]	R_1 = 0.1407, wR_2 = 0.2040
largest diff. peak/hole / e Å^{-3}	0.92/-0.70

Table S4. Selected bond distances (Å) and bond angles (°) for **PCP-35**.

Bond Distances (Å)			
Zn1—O7	1.972 (5)	Zn4—O14^{iii}	1.946 (4)
Zn1—O15^{i}	2.487 (7)	Zn4—N11^{iv}	2.179 (5)
Zn1—O16^{i}	2.165 (8)	Zn4—N12^{iv}	2.074 (4)
Zn1—N7	2.181 (7)	Zn4—N13^{iv}	2.150 (5)
Zn1—N8	2.059 (5)	P1—O1	1.580 (3)
Zn1—N9	2.144 (7)	P1—O2	1.592 (3)
Zn2—O8	1.972 (4)	P1—N1	1.580 (4)
Zn2—O9	1.923 (4)	P1—N2	1.571 (4)
Zn2—N15^{ii}	2.052 (5)	P2—O5	1.590 (3)
Zn2—N14^{ii}	2.210 (5)	P2—O6	1.586 (3)
Zn2—N10^{ii}	2.118 (5)	P2—N2	1.564 (4)
Zn3—O13	1.969 (4)	P2—N3	1.583 (4)
Zn3—O17	1.900 (4)	P3—O3	1.579 (4)
Zn3—N4	2.146 (5)	P3—O4	1.576 (4)
Zn3—N5	2.039 (4)	P3—N1	1.561 (4)
Zn3—N6	2.149 (6)	P3—N3	1.566 (4)
Zn4—O12	1.952 (4)		
Bond Angles (°)			
O7—Zn1—O15^{i}	133.0 (2)	N4—Zn3—N6	152.83 (18)
O7—Zn1—O16^{i}	83.0 (3)	N5—Zn3—N4	76.3 (2)
O7—Zn1—N7	88.2 (2)	N5—Zn3—N6	76.57 (19)
O7—Zn1—N8	124.5 (2)	O12—Zn4—N11^{iv}	91.70 (19)
O7—Zn1—N9	109.2 (2)	O12—Zn4—N12^{iv}	112.93 (16)
O16^{i}—Zn1—O15^{i}	55.6 (2)	O12—Zn4—N13^{iv}	108.70 (18)
O16^{i}—Zn1—N7	111.4 (4)	O14^{iii}—Zn4—O12	104.24 (17)
N7—Zn1—O15^{i}	87.6 (2)	O14^{iii}—Zn4—N11^{iv}	103.60 (18)
N8—Zn1—O15^{i}	99.2 (2)	O14^{iii}—Zn4—N12^{iv}	142.79 (17)
N8—Zn1—O16^{i}	152.4 (3)	O14^{iii}—Zn4—N13^{iv}	95.38 (17)
N8—Zn1—N7	74.8 (2)	N12^{iv}—Zn4—N11^{iv}	74.43 (18)
N8—Zn1—N9	75.5 (3)	N12^{iv}—Zn4—N13^{iv}	74.73 (17)
N9—Zn1—O15^{i}	96.7 (2)	N13^{iv}—Zn4—N11^{iv}	147.81 (17)
N9—Zn1—O16^{i}	94.9 (4)	O1—P1—O2	98.32 (19)
N9—Zn1—N7	150.3 (2)	N1—P1—O1	110.9 (2)
O8—Zn2—N15^{ii}	148.31 (19)	N1—P1—O2	111.6 (2)
O8—Zn2—N14^{ii}	103.28 (19)	N2—P1—O1	111.3 (2)
O8—Zn2—N10^{ii}	94.3 (2)	N2—P1—O2	106.3 (2)
O9—Zn2—O8	101.71 (18)	N2—P1—N1	116.7 (2)
O9—Zn2—N15^{ii}	109.85 (17)	O6—P2—O5	94.28 (17)
O9—Zn2—N14^{ii}	90.78 (17)	N2—P2—O5	110.7 (2)
O9—Zn2—N10^{ii}	113.44 (17)	N2—P2—O6	112.2 (2)
N15^{ii}—Zn2—N14^{ii}	74.08 (19)	N2—P2—N3	117.3 (2)
N15^{ii}—Zn2—N10^{ii}	76.1 (2)	N3—P2—O5	110.8 (2)
N10^{ii}—Zn2—N14^{ii}	146.57 (19)	N3—P2—O6	109.3 (2)
O13—Zn3—N4	95.16 (19)	O4—P3—O3	99.9 (2)
O13—Zn3—N5	110.98 (16)	N1—P3—O3	112.4 (2)

O13—Zn3—N6	92.44 (19)	N1—P3—O4	109.4 (2)
O17—Zn3—O13	107.79 (17)	N1—P3—N3	118.3 (2)
O17—Zn3—N4	99.50 (18)	N3—P3—O3	104.4 (2)
O17—Zn3—N5	141.22 (17)	N3—P3—O4	110.8 (2)
O17—Zn3—N6	102.93 (19)		

Symmetry codes: (i) −*x*+2, −*y*, −*z*+1; (ii) −*x*+2, −*y*+1, −*z*; (iii) −*x*+1, −*y*, −*z*+1; (iv) *x*+1, *y*, *z*−1.

Table S5. The lifetimes of **PCP-35** and analytes.

Lifetime (ns)	Sample
0.049625 ns	**PCP-35**
0.047322 ns	**PCP-35+BA**
0.045673 ns	**PCP-35+SA**
0.044791 ns	**PCP-35+FA**

Table S6. Comparison of aldehyde vapour sensing of **PCP-35** with representative Zn-based and phosphazene-related MOFs.

Material	Metal	Ligand Type	Structure	Application	Performance	Ref
Compound 1	Ln(III)	Cyclotriphosphazene hexacarboxylate	3D	Aldehyde sensing	SA ↑ (~24%), FA quenching (>50%), BA ~ no response	[11]
Zn-adtb (LMOF-341)	Zn(II)	Carboxylate	3D	VOC sensing	Moderate sensitivity (Ksv ~10^2 M^{-1})	[12]
ZnCo(NA)	Zn/Co	Nicotinic acid	Microporous	VOC sensing	Response ≈ 28.3 (HCHO)	[13]
MOF-derived ZnO	Zn	BTC-derived	Derived	VOC sensing	LoD ~100 ppb	[14]
PCP-35	**Zn(II)**	**Cyclotriphosphazene + bisterpyridine**	**3D π-stacked**	**Dual (photocatalysis + sensing)**	**>90% degradation + selective aldehyde sensing**	**This work**

Table S7. Comparison of dye degradation of **PCP-35** with representative Zn-based and phosphazene-related MOFs.

Coordination Polymer/MOF	**Dye**	**Light Source**	**Time (min)**	**Degradation (%)**	**Ref.**
$[Zn(tpbpc)(bdc)_{0.5}\cdot H_2O]\cdot$solvent	MO	Visible light	90	100	[15]
$Zn_4O(2,6\text{-}NDC)_3\cdot(DMF)\cdot1.5(H_2O)\cdot0.54DMF\cdot7.5H_2O$	MO	Visible light	180	65	[16]
$[Zn_4(2\text{-}mim)6WO_4]\cdot1.5DMF$ (HZIF-1W)	$MO(H_2O_2)$	Visible light	120	24.5	[17]
$[Zn_4(2\text{-}mim)6MoO_4]\cdot2DMF$ (HZIF-1Mo)	$MO(H_2O_2)$	Visible light	120	81.6	[17]
$[(Zn(L)(hip))\cdot2H_2O]n$	MO	UV	150	61	[18]
PCP-10	MB / RhB / MO	UVA	60	~90	[19]
PCP-18	MB	Full spectrum	90	>90	[1]
PCP-35	**MB**	**Visible light**	**40**	**95**	**This work**
PCP-35	**RhB**	**Visible light**	**60**	**90**	**This work**
PCP-35	**MO**	**Visible light**	**60**	**92**	**This work**

References

1 Pendar A., Özcan E., Yatmaz H. C., Zorlu Y., (2025). Multifunctional Anionic Cyclotriphosphazene-Based Metal–Organic Framework Featuring a One-Dimensional Zn(II) Inorganic Building Unit for Selective Chemical Sensing and Efficient Photocatalytic Activity. *Crystal Growth & Design*, 25 (15), 6169–6182.

2 SAINT, version 8.34A, Bruker AXS Inc., Madison, WI, 2013.

3 APEX2, version 2014.11-0, Bruker AXS Inc., Madison, WI, 2014.

4 SADABS, version 2014/5, Bruker AXS Inc., Madison, WI, 2014.

5 G.M. Sheldrick, *Acta Crystallogr. A* 2015, *71*, 3–8.

6 G.M. Sheldrick, *Acta Crystallogr. C* 2015, *71*, 3–8.

7 O.V. Dolomanov, L.J. Bourhis, R.J. Gildea, J.A. Howard, H. Puschmann, *J. Appl. Crystallogr*. 2009,

42, 339–341.

8 A.L. Spek, *Acta Crystallogr. C* 2015, *71*, 9–18.

9 Blatov V. A., Shevchenko A. P., Proserpio D. M., (2014). Applied Topological Analysis of Crystal Structures with the Program Package ToposPro. *Crystal Growth & Design*, 14 (7), 3576–3586.

10 Constable E. C., Cargill Thompson A. M. W., (1992). Multinucleating 2,2′:6′,2″-Terpyridine Ligands as Building Blocks for the Assembly of Coordination Polymers and Oligomers. *Journal of the Chemical Society, Dalton Transactions*, 1992, 3467–3475.

11 Yu S., Li J. X., Zeng G., Xing Y. H., Bai F. Y., Shi Z., (2022). Construction of Large-Scale Conjugated Functionalized Cyclotriphosphazene Lanthanide Framework for Selective Sensing of Volatile Organic Compounds and Assembly of Color-Tunable Dye-Encapsulated Composites. *Inorganic Chemistry*, 61, 3111–3120.

12 Velasco E., Zhang G., Teat S. J., Tan K., Ullah S., Thonhauser T., Li J., (2023). Luminescent Metal–Organic Framework for the Selective Detection of Aldehydes. *Inorganic Chemistry*, 62, 16435–16442.

13 Reddy A. J. M., Suresh K., Benarzee N. S., Babu M. S. S., (2023). Synthesis and Characterization of Zn-Based Bimetallic Microporous MOF Composites for Effective Formaldehyde Sensing at Room Temperature. *Inorganic Chemistry Communications*, 158, 111612.

14 Ling W., Zhu D., Pu Y., Li H., (2022). The ppb-Level Formaldehyde Detection with UV Excitation for Yolk–Shell MOF-Derived ZnO at Room Temperature. *Sensors and Actuators B: Chemical*, 355, 131294.

15 Liu J., Xiao J., Wang D., Sun W., Gao X., Yu H., Liu Z., (2017). Construction and photocatalytic activities of a series of isostructural Co^{2+}/Zn^{2+} metal-doped metal– organic frameworks. *Crystal Growth & Design*, 17 (3), 1096–1102.

16 Das M. C., Xu H., Wang Z., Srinivas G., Zhou W., Yue Y. F., Chen B., (2011). A Zn_4O-containing doubly interpenetrated porous metal–organic framework for photocatalytic decomposition of methyl orange. *Chemical Communications*, 47 (42), 11715–11717.

17 Wang F., Liu Z. S., Yang H., Tan Y. X., Zhang J., (2011). Hybrid zeolitic imidazolate frameworks with catalytically active TO_4 building blocks. *Angewandte Chemie*, 123 (2), 470–473.

18 Wang G. L., Wang J., Zhou L. P., Cai X., Xu M., Lin J., Sakiyama H., (2021). A multi-functional Cd(II)-based coordination polymer for the highly sensitive detection of nitrofurazone and photocatalytic efficiency of Rhodamine B. *Inorganica Chimica Acta*, 527, 120566.

19 Özcan E., Kartal A. N., Yatmaz H. C., Zorlu Y., (2025). Two-Dimensional-Layered Zn(II) Cyclophosphazene–Organic Framework for Effective Photocatalytic Removal of Organic Dyes. *Applied Organometallic Chemistry*, 39 (4), e70080.